Turbulence characteristics of the Martian atmosphere surface layer based on Zhurong observations

Mengling Yang[1], Renmin Yuan[1*], Hao Liu[2], Tao Li[1,3,4*], Jun Yang[5], and Yongyun Hu[5]

[1] School of Earth and Space Sciences, University of Science and Technology of China, Hefei, Anhui, China.

[2] School of Mathematics & Physics, Anhui Jianzhu University, Hefei, Anhui, China.

[3]CAS Key Laboratory of Geospace Environment, School of Earth and Space Sciences, University of Science and Technology of China, Hefei, China.

[4]CAS Center for Excellence in Comparative Planetology, University of Science and Technology of China, Hefei, China.

[5] School of Atmosphere and Ocean Sciences, Peking University, Beijing, China

Key Points:

- The two-dimensional temperature spectrum at the Zhuong location displays four wave peaks.
- The temperature and refractive index structure parameters have significant geographical variability.
- The heat flux at the Zhurong and Insight locations was lower than at the Perseverance location.

* Correspondence to: Renmin Yuan (rmyuan@ustc.edu.cn) and Tao Li (litao@ustc.edu.cn)

Abstract

Studying the Martian atmosphere is important in planetary science. The boundary layer turbulence is characterized at the Zhurong location using spectrum analysis, two-dimensional spectrum, and similarity theory. The results reveal that the atmospheric temperature and wind at the Zhurong location are consistent with Kolmogorov's "-5/3" turbulence laws. The atmospheric movement at the Zhurong location has four usual weather scales: 50 m, 100 m, 150 m, and 200 m. The atmospheric refractive index structure parameters, and thus the effect of turbulence on the light propagation, at the Zhuong and Insight locations are 3 or 4 orders less than at the Perseverance location. The sensible heat flux values in the Zhurong location is mainly in the range of 0-10 W/m²and increases during measurement. The clear seasonal variability in heat flux flow with greater value in spring and summer than in autumn and winter is revealed at both the Zhuong and Insight locations.

Plain Language Summary

Mars is an important area for deep space exploration. The surface layer of Mars is the region directly explored by the rover, and understanding the characteristics of its atmospheric environment is critical for future rover landings.This study characterises surface turbulence in terms of scale, intensity, and heat transport. The study found that the outer scale of turbulence on Mars is about 30m. Four scales of weather systems may affect surface layer temperatures, their scales are 50 m, 100 m, 150 m, and 200 m. Combining Perseverance and Insight Mars rover data, geographical variations affect the intensity of turbulence, which also shows seasonal variations. This difference in magnitude can make the impact on optical transmission vary from region to region. Turbulence due to buoyancy differences causes variability in surface heat flux. However, the sensible heat fluxes of both Zhurong and Insight locations have a seasonal trend, with the trend being higher values in spring and summer than in autumn and winter. These results are important for deepening human understanding of Mars.

1 Introduction

The boundary layer acts as a medium for exchanging energy and matter between the surface and the free atmosphere on both Mars and Earth. Using large eddy simulations, Gheynani found that the Martian boundary layer is approximately six times higher than Earth's, with more turbulent activity(Gheynani & Taylor, 2011). Richard Davy et al. calculated a wind speed-normalized turbulence spectrum at the Phoenix location consistent with the Kolmogorov turbulence "-5/3" law(Davy et al., 2010), and Petrosyan et al. (2011) reached similar conclusions using large eddy simulations and data from the Viking 2 and Phoenix rover observations. Earth and Mars have nearly identical turbulence laws and very similar nonlinear dynamics and are fully turbulent over most scale ranges(Chen et al., 2016). Martínez et al. (2009) calculated the local heat flux for a single day using data from Pathfinder. Because of measurement limitations, studies of Martian turbulence are still relatively rudimentary, with very few quantitative descriptions of turbulence in terms of scales and intensity. Besides spectrum characterization, the turbulence structure parameters quantify small-scale turbulence. Turbulence affects electromagnetic wave propagation in the atmosphere. The variation of refractive index structure parameters on Mars reflects this process. Thus, more Mars observation experiments are needed to understand the fundamental principles of the Martian atmosphere. This study examines the turbulent structure parameters of the Martian atmosphere in the surface layer. It also investigates

Mars's atmospheric movement scales and seasonal turbulent transport regulations in the surface layer.

Since the 1960s, more than twenty Mars exploration projects have used at least five rovers for meteorological observations (Banfield et al., 2020; Davy et al., 2010; Lemmon et al., 2015; Seiff et al., 1997). The Zhurong data enriches Mars' surface observation datasets. This paper uses meteorological data from Zhurong's meteorological measurements to study surface turbulence at the Utopia Plain landing site.

2 Data and Analysis Methods

2.1 Data

On May 15, 2021, the Zhurong landed successfully in the Utopia Plains at 109°E and 25.1°N. The rover is 1.85 meters tall and equipped with the Mars Meteorological Measuring Instrument. The rover recorded 1 Hz temperature, pressure, and wind data.

Comparing and analyzing data from the Perseverance and Insight near the Zhurong will help us better understand the Martian surface. On 18 February 2021, the Perseverance successfully landed in Jezero crater lake at 77.5°E and 18.4°N. The rover is 2.2 meters high. The data included temperature, pressure and wind. Unfortunately, wind measurements have been lost since Sol 315. According to the Mars Orbiter Laser Altimeter(MOLA) elevation map(Smith et al., 2001), Zhurong's elevation is 1535 m lower than that of Perseverance. The two rovers differ by 6.7° in latitude and 31.5° in longitude. On 26 November 2018, Insight landed near the Martian equator at 135.6°E, 4.5°N. The station has consistently recorded surface pressure, temperature and wind for almost a full Martian year. In this article, the name of the Mars Rovers is used to refer to their landing location.

On Mars days, Zhurong's instruments started measuring at 09:45 or 09:16 and collected data for 41 to 50 minutes. While the instruments on Perseverance and Insight have a continuous measurement period that spans the entire day, each individual measurement lasts one hour. In addition, sampling intervals and collection times for different elements vary. Therefore, this paper mainly emphasizes the temporal variations in the average field between 9:00 a.m. and 10:00 a.m.

2.2 Power spectrum method

The power spectral density $F_T(f)$ for temperature (or velocity) fluctuations satisfies the "-5/3" law(Wyngaard et al., 1971) and is represented in frequency coordinates as:

$$F_T(f) = (2\pi/U)F_T(\kappa) = 0.25C_T^2(2\pi/U)^{-2/3} f^{-5/3} \quad (1)$$

where κ is the wavenumber, U is the mean wind speed, and C_T^2 is a temperature structure parameter used to characterize the intensity of small-scale temperature fluctuations.

2.3 Conversion of the two-dimensional spectrum

The spatial spectrum distribution of atmospheric turbulence provides scale information. Since the three-dimensional movement of the atmosphere, the one-dimensional(1-D) spectrum could underestimate the wave peak and related scale of information. Still, the three-dimensional spectrum is impossible to obtain. A two-dimensional spectrum can better reflect scale

information under realistic situations. If atmospheric motion is statistically isotropic, the 1-D spectrum can be converted into a two-dimensional(2-D) spectrum for better spatial scale information(Kelly & Wyngaard, 2006) .

Equation (1) converts the frequency spectrum *F(f)* to a 1-D *F(κ)*, and then the 2-D spectrum *E(κh)* is(Kelly & Wyngaard, 2006)：

$$E(\kappa_h) = \frac{d}{d\kappa_h}\int_{\kappa_h}^{+\infty} \frac{2\kappa F(\kappa)}{(\kappa^2 - \kappa_h^2)^{1/2}} d\kappa \tag{2}$$

2.4 Refractive Index Structure Parameters

The previous part converts a 1-D spectrum into a 2-D spectrum to collect turbulence scale information. We also focus on turbulence intensity, which can be measured using the temperature structure parameter C_T^2 (Belov et al., 2012). To determine how atmospheric turbulence affects light propagation, the temperature structure parameter C_T^2 should be used to calculate the refractive structure parameter C_n^2.

Cahoy's Mars refractive index calculation formula(Cahoy et al., 2006)can be used in conjunction with the gas state equation to approximate the relationship between the refractive index structure parameter and the temperature structure parameter:

$$C_n^2 = (\frac{vp}{RT^2} N_A)^2 C_T^2 \tag{3}$$

2.5 Surface turbulent transport

Atmospheric turbulence plays a critical role in the surface layer of Mars by transporting materials, energy, and momentum between the Martian surface and the atmosphere. Within the surface constant flux layer, the sensible heat flux of the turbulent vertical flux can be expressed as:

$$F_h = c_p \rho_0 \overline{T'w'} = -c_p \rho_0 u_* T_* = const \tag{4}$$

where T' and w' represent the temperature and vertical velocity fluctuation terms, respectively. Characteristic temperature T_* and friction velocity u_*. According to the similarity theory, the wind speed at height z can be expressed as

$$U(z) = \frac{u_*}{k}[\ln(\frac{z}{z_0}) - \psi(\frac{z}{L})] \tag{5}$$

where z_0 is the roughness, and L is the Obukhov length(Obukhov, 1971), which characterizes the surface layer stability and is defined as:

$$L = \frac{\bar{T} u_*^2}{kgT_*} \tag{6}$$

where g is taken as 3.72 m s^{-2}, k is the von Karman constant of 0.4, and $\bar{T}$ is the average wind speed. $\psi(\frac{z}{L})$ is the correction term, denoted as(Petrosyan et al., 2011):

$$\psi(\frac{z}{L}) = 2\ln(\frac{1+x}{2}) + \ln(\frac{1+x^2}{2}) - 2\tan^{-1}x + \frac{\pi}{2}, \frac{z}{L} < 0$$
$$\psi(\frac{z}{L}) = -c\ln\{\frac{z}{L} + [1 + (\frac{z}{L})^d]^{1/d}\}, \qquad \frac{z}{L} \geq 0 \tag{7}$$

where $x = (1 - \gamma_1 \frac{z}{L})^{1/4}$, γ_1=16, c=5.3, and d=1.1(Cheng & Brutsaert, 2005).

When the layer junction is in convective instability, the stability parameter basically satisfies 0.03<-z/L<60, and the temperature fluctuation square can be expressed as:

$$\frac{\sigma_T}{T_*} = C_1(C_2 - \frac{z}{L})^{-1/3} \tag{8}$$

where C_1=0.95 and C_2=0.0549. Under the free convection assumption, the equation can be simplified to:

$$\frac{\sigma_T}{T_*} = C_1(-\frac{z}{L})^{-1/3} \tag{9}$$

In summary, based on Eqs. (4), (5), and (9), the heat flux during a certain period can be calculated via an iterative method(Petrosyan et al., 2011).

T_* and u_* can also be used to calculate the turbulent momentum diffusion coefficient *km* and turbulent heat diffusion coefficient *kh* in the boundary layer model(Martínez et al., 2009):

$$\overline{u'w'} = -u_*^2 = -k_m \frac{\partial U}{\partial z} = k_m \frac{u_*}{kz}\phi_m(\frac{z}{L})$$
$$\overline{T'w'} = -u_*T_* = -k_h \frac{\partial T}{\partial z} = k_h \frac{T_*}{kz}\phi_h(\frac{z}{L}) \tag{10}$$

The generic functions ϕ_m and ϕ_h are derived from Högström(Hogstrom, 1988).

3 Results and discussion

We first discuss the fluctuation characteristics of the average surface temperature and pressure in Zhurong. This is followed by air temperature, wind speed, and pressure variability, including power spectrum variability, scale obtained from spectrum analysis, and variability in turbulence intensity. We also compare the characteristics of the surface layers in the vicinity of the Perseverance and Insight sites.

3.1 Conventional meteorological data

First, the morning seasonal meteorological trends at the three sites were compared. Figure 1(a) shows that the Zhurong result had a higher average temperature than Perseverance and Insight during the morning. Perseverance and Insight results slightly linearly increased in summer but slowly decreased in autumn, and stabilized in winter and spring. The seasonal variation in pressure is strongly influenced by altitude, as shown in Fig. 1(b). The pressure at all three locations also follows similar seasonal trends. They rise slightly in spring and fall slowly in summer, reaching their lowest point at 135°solar longitude. They then gradually increase during the autumn, reaching their highest point at 240° solar longitude. During the winter, they slowly

decrease. Figure 1(c) shows the wind speed for the three locations. The wind speeds were less than 6 m/s for Zhurong and Perseverance and more than 4 m/s for Insight. There were also clear seasonal variations in wind speed. The wind speed showed a progressive increase over the summer, followed by a gradual decrease in the autumn. However, the wind speed trends became more erratic in winter and spring.

We also compared the same 4 consecutive days of weather for Zhurong and Perseverance. The results are shown in Figure 1(d)(e). In the morning, Zhurong has an average pressure of 701 Pa and an average temperature of 248.5 K, while Perseverance has a pressure of 653 Pa with a difference of 48 Pa and a temperature of 232 K. The model proposed by Chen et al. estimates the Martian atmospheric density at 223 K at approximately 7×10^{-3} kg/m^3(Chen et al., 2016). According to the pressure-height equation, a height difference of 1535 m results in a pressure difference of roughly 42 Pa. The calculated pressure difference between the two locations is very close. Differences in geographical position can influence the horizontal pressure difference.

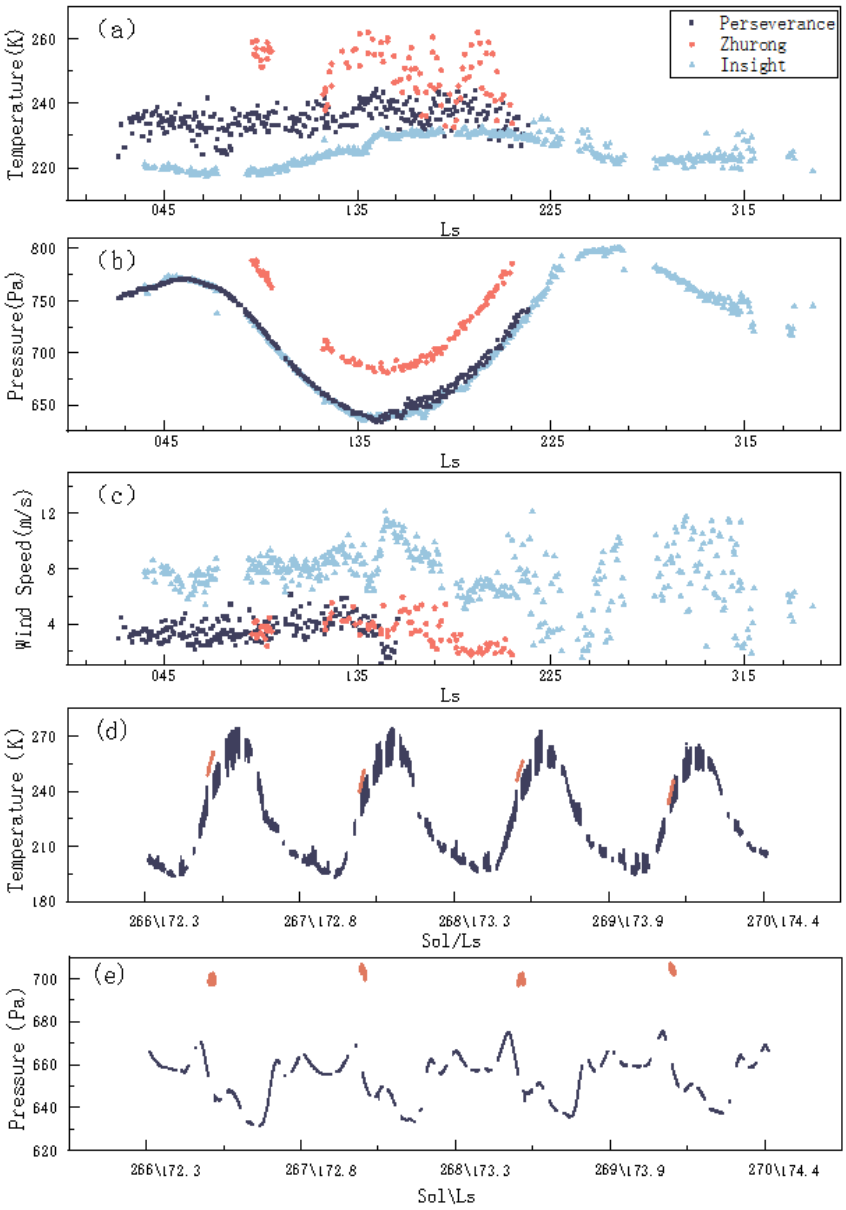

Fig. 1 Seasonal fluctuations in **(a)** temperature, **(b)** pressure, and **(c)** wind speed. The time series for the Sol 266-Sol 269 measurements of **(d)** temperature and **(e)** pressure. where red is Zhurong, dark blue is Perseverance, and light blue is Insight

3.2 Turbulence Characterization

Turbulence characteristics are generally quantified from two perspectives: the turbulence scale and turbulence intensity. First, we confirm that Martian atmospheric turbulence follows turbulence laws. Scale information is obtained using 2-D spectral methods. To characterize the intensity of the turbulence, the temperature structure parameter and the refractive index structure parameter were calculated.

3.2.1 Turbulence Spectrum and Turbulence Scale

Understanding the scale of turbulence is important for assessing its properties, as it dominates boundary layer gas motion. Figures 2(a), (c), and (e) show the time variation of temperature, pressure, and wind speed, respectively. The ambient temperature can be determined from the temperatures at three specific points on the PCB temperature frame(Peng et al., 2020). t_1 has more high-frequency components. This makes it more suitable for studying turbulence characteristics. There are six significant pressure variations. The wind speed changes follow a clear pattern of periodic variations every 5 minutes.

It is important to transform the time series into a power spectrum to obtain the high-frequency variability and scale information of atmospheric motion. The usual processing approach is to multiply the power spectrum density(PSD) by the frequency, and the results for Sol 269 are shown in Figs 2(b), (d), and (f). In the range of 0.01~0.1 Hz, the smooth line of temperature and wind speed matches the trend of the "-3/2" line, indicating that Kolmogorov's theory of turbulence still applies on Mars. Studies by Petrosyan et al. have reached the same conclusion(Petrosyan et al., 2011). Increasing pressure at higher frequencies flattens the power spectrum fit away from the expected "-3/2" line. However, in the lower frequency range, the smooth line is consistent with the fit and has similar characteristics to the high-pressure spectrum. The results obtained are inconsistent with the theoretical predictions of Kolmogorov's theory of the PSD of pressure fluctuations, which is expected to have a scaling exponent of -7/3(Banfield et al., 2020).

The turbulent outer scale divides the atmospheric scale into two distinct regions. The vortices smaller than the outer scale are isotropic, and those beyond the outer scale are affected by other weather systems, resulting in an anisotropic state. Temperature variations are important in determining how turbulence develops. Identifying the outer scale requires screening the temperature spectrum for deviations from the turbulence law. The coordinates of the first peak point outside the confidence interval in Fig. 2b indicate that the outer scale is about 30 m at this time. In addition to the turbulent outer scales, we also revealed the presence of other peaks in the power spectrum. These peaks correspond to wavelengths of 48 m, 70 m, 107 m, and 231 m, respectively. Furthermore, it is worth noting that the calculated outer scale of the wind speed spectrum remains at 30 m, which is consistent with the outer scale based on the temperature spectrum. In addition, the power spectrum of the wind speed has a clear discontinuity in the waveforms on both sides at a frequency of 0.01 Hz. There is speculation about the possible combined influence of at least two weather systems on wind speed, leading to the observed truncation after power spectrum superposition.

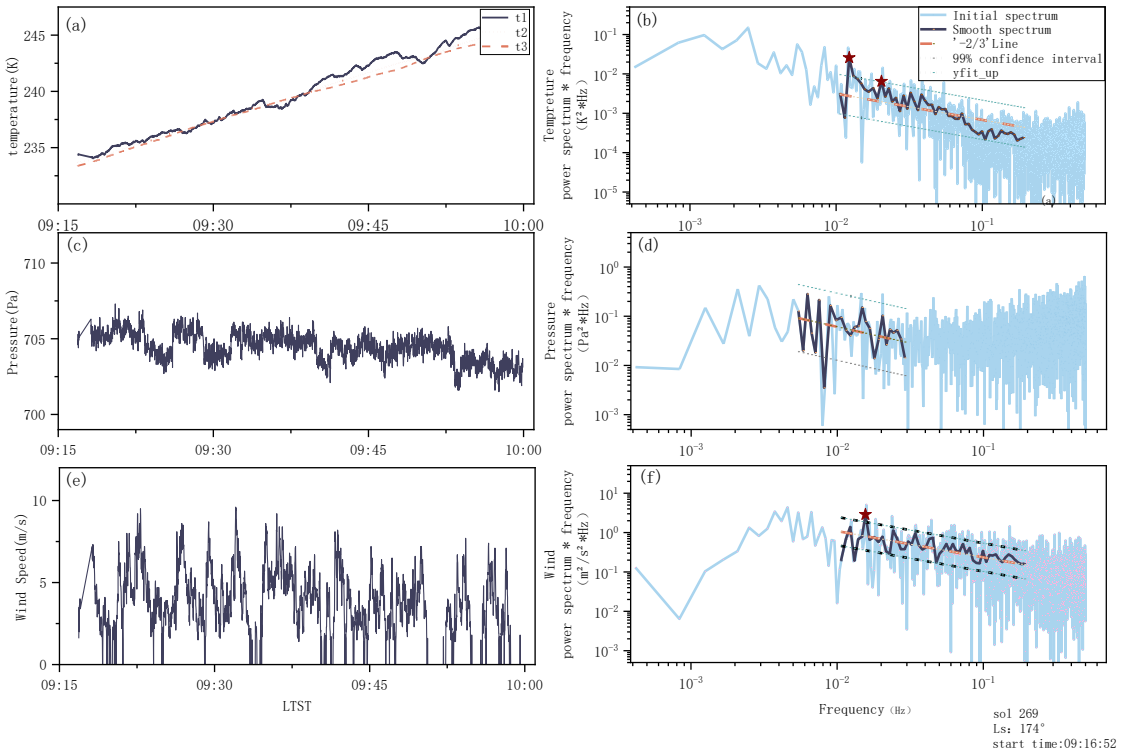

Fig. 2 The time series of **(a)** temperature, **(c)** pressure, and **(e)** wind speed; frequency · power spectrum of **(b)** pressure, **(d)** temperature, and **(f)** wind speed for Sol 269

Even after smoothing, a 1-D spectrum still contains many peaks and needs to be transformed into a 2-D spectrum to identify typical scaling further. The results for partial days are shown in Fig. 3. The statistics show the presence of four distinct peaks at heights of 30 m, 50 m, 100 m, and 250 m. Through statistical analysis of a dataset spanning 75 days, the wave peak with a length of 30 m fluctuated 52 times, the wave peak with a length of 50 m fluctuated 41 times, the wave peak with a length of 100 m fluctuated 26 times, and the wave peak with a length of 250 m fluctuated 14 times. Furthermore, the 2-D temperature spectrum is not limited to the abovementioned four scales. Sometimes the wind speed can have an influence, and the 2-D spectrum of the temperature shows a state of three to five peaks.

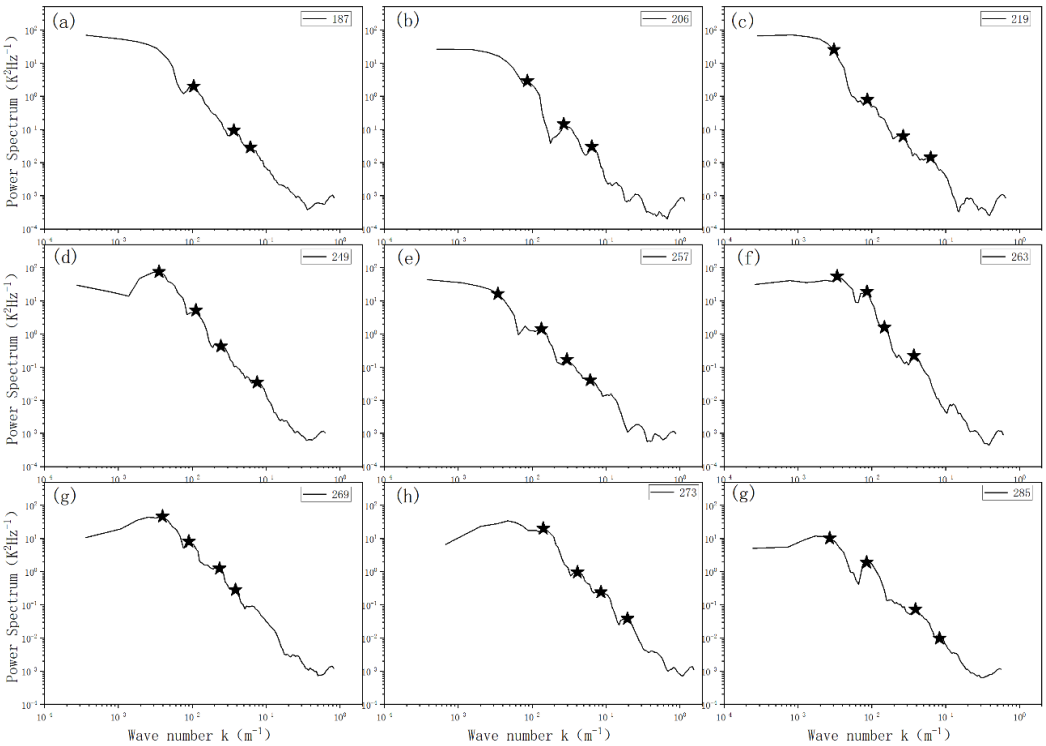

Fig. 3 2-D spectrum of the temperatures for multiple Martian days

3.2.2 Temperature and refractive index structure parameters

Another crucial metric for characterizing the turbulence field is the turbulence intensity, measured in addition to the turbulence scale. Figure 4 shows that the mean refractive index structure parameter of the atmosphere measured by Zhurong is 4.6×10^{-19} $m^{-2/3}$, while the Perseverance is 6.6×10^{-16} $m^{-2/3}$. During the spring and summer, when the sun's longitude is less than 180°, the average Insight is 9.7×10^{-19} $m^{-2/3}$. At angles greater than 180°, the average value is approximately $.6\times10^{-18}$ $m^{-2/3}$. Both the temperature structure parameter and the refractive index structure parameter exhibit distinct seasonal variations, remaining relatively constant during spring and summer, decreasing during fall, and significantly exceeding the levels observed in spring and summer during winter. Simultaneously, we observed notable variations in the magnitudes of the refractive index structure parameters among the three locations. The Perseverance exhibits the most turbulence intensity, followed by the Insight, while the Zhurong area experiences the lowest turbulence. The regional disparity may be attributed to the spatial distribution of the Martian atmosphere, as well as the distributions of radiation flow and sensible heat flux.

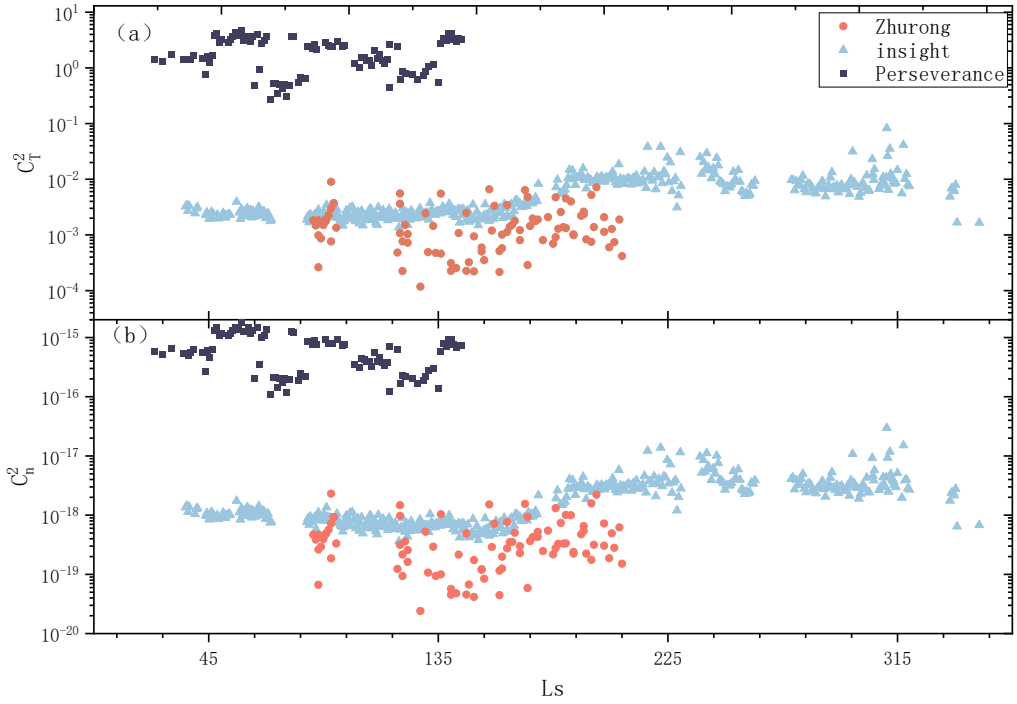

Figure 4 Variations in the (a) temperature structure parameter **and (b)** refractive index structure parameter, where red is Zhurong, dark blue is Perseverance, and light blue is Insight

3.3 Surface heat flux and turbulent diffusion coefficients

The study of heat transport caused by turbulence is important in characterizing the turbulence field. Turbulent conditions are generated by buoyancy and shear mechanisms. This phenomenon can be quantified more precisely using the friction velocity, u_*, the characteristic temperature, T_*, and the Obukhov length, L.

As displayed in Fig. 5(a), the friction velocity u_* of Perseverance remains fairly stable at approximately 0.2-0.4 m/s. The friction velocity u_* of Zhurong is identical to that of Perseverance before a solar longitude of 150°; however, it decreases progressively to approximately 0.2 m/s thereafter. The value of Insight was 0.3 m/s. Zhurong's absolute T_* is lower than that of Perseverance, while the values and trends of Insight are shown in Fig. 5(b). The magnitude of T_* represents the influence of buoyancy. While the calculation results are impacted by the temperature variation, the aforementioned error in the temperature variation on T_* has a negligible effect, fluctuating by less than 0.4% or approximately 0.001 K. As shown in Fig. 5(c), the Obukhov length at Zhu Rong consistently varies between -10^2 and -10^1 m. The L values at the three sites are not significantly different, and this calculation is comparable to that of Petropsyan et al.(Banfield et al., 2020). Specifically, Zhurong's calculations are almost identical.

Overall, the atmosphere at all three locations was unstable between 9 a.m. and 10 a.m., which promoted the formation of turbulence. The speed scales for all three locations were essentially identical; however, Zhurong and Insight had smaller buoyancy effects than Perseverance, resulting in weaker vertical transport.

The turbulent diffusion coefficient values *km* and *kh* often express the magnitude of turbulent momentum and heat fluxes in boundary layer atmospheric models. Typically, the molecular heat diffusivity and molecular kinematic viscosities are on the order of 10^{-3} m^2s^{-1}. The turbulent diffusion efficiency on Mars was approximately two orders of magnitude greater than the molecular diffusion efficiency. The *km* m in all three places was 0.3 m^2s^{-1}. The *kh* values from smallest to largest were 0.32 m^2s^{-1} for Zhurong, 0.37 m^2s^{-1} for Insight, and 0.45 m^2s^{-1} for Perseverance.

The variation in heat flux with solar longitude was calculated at the three sites, as shown in Fig. 9(d). The heat flux in Zhurong ranges from 0 to 10 W/m². During the same season, the heat flux of Insight is comparable to that of Zhurong; however, it is greater in autumn and winter than in spring and summer. The heat flux in Zhurong is lower than that in Perseverance.

Much of this difference is caused by turbulence. The surface heat flow is mainly determined by the correlation between the vertical velocity and temperature variations. In contrast, buoyancy generates turbulence due to the upward sensible heat flow at the planet's surface. The vertical velocity variation is typically less dramatic than the temperature variation, so the heat flux and variation range in the weaker vertical transport Zhurong will be smaller than those throughout the Perseverance. Furthermore, the altitude difference may be a factor for the large difference between the two heat fluxes. According to Haberle et al., the effect of longwave radiation explains why the heat flux of Viking 1 in the Golden Plain at a higher altitude is greater than that of Viking 2 in the Utopia Plain(Haberle et al., 1993).

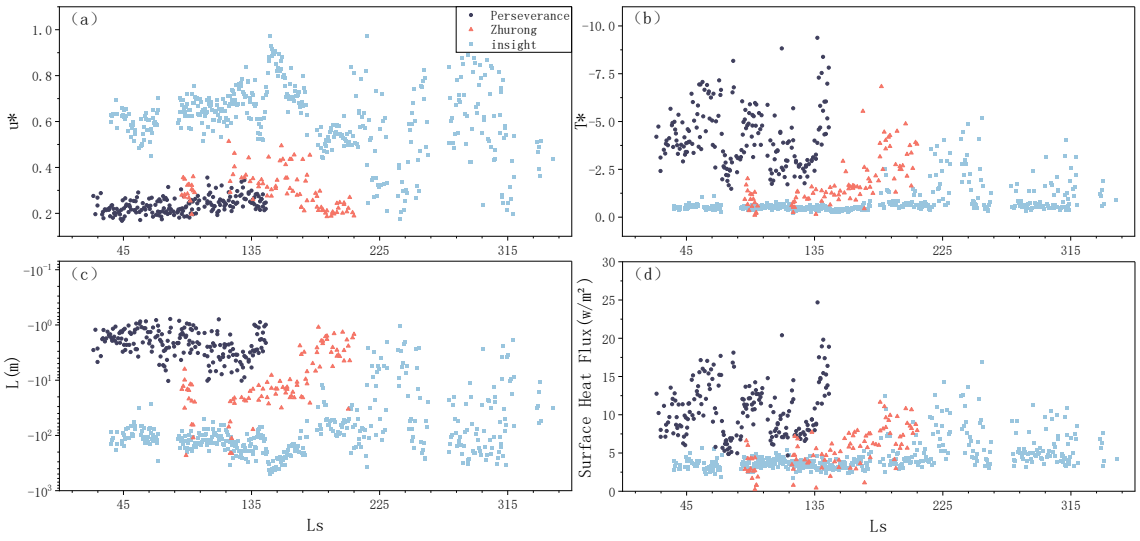

Fig. 5 (a) Friction velocities u_*, **(b)** characteristic temperature T_*, **(c)** Obukhov lengths L and **(d)** the heat flux, where the red is Zhurong, the dark blue is Perseverance, and the light blue is Insight

4 Conclusions

The following conclusions are derived from the research:

(1) The turbulence "-5/3" law of temperature and wind speed remains valid for the Martian boundary layer. The wind power spectrum discontinuity phenomenon was also identified, but its cause and mechanism are unclear.

(2) The 2-D temperature spectrum of Zhurong shows four peaks at 30 m, 50 m, 100 m and 250 m. The atmospheric temperature structure parameter and the refractive index structure parameter have geographical variations, and three to four orders of magnitude separate the values of Zhurong and Insight from Perseverance. This turbulence in the Perseverance has a greater effect on light transmission than does the turbulence in the Zhurong and Insight values.

(3) The heat fluxes in Zhurong and Insight were lower than that in Perseverance. The disparity in question may stem from the influence of buoyancy on the ability to vertically transfer, as well as the variation in longwave radiation. However, deeper mechanisms affecting heat flux need to be analyzed with more diverse data.

Acknowledgments: We thank the Tianwen-1 engineeringteam for such a successful mission, payload team for mission operations and China National Space Administration (CNSA) for providing the Tianwen-1 scientific data that made this study possible. **Funding:** The work described in this paper was carried out at the University of Science and Technology of China under the support of the B-type Strategic Priority Program of the Chinese Academy of Sciences Grant No. XDB41000000, and the National Natural Science Foundation of China grants 42130203. **Author contributions:** Design and lead of this research: R.Y and T.L. Conceptualization: J.Y. and Y.H. Data processing: M.Y. and R.Y. Methodology: R.Y., M.Y., H.L. and T.L. Writing: M.Y., T.L. and R.Y. **Competing interests:** The authors declare that they have no competing intrests. **Data Availability Statement:** The data reported in this work are publicly available at the Lunar and Planetary Data Release System (https://moon.bao.ac.cn/web/enmanager/home. Path to access the data: Home Page>Scientific Data>Mars) and NASA's Planetary Data System (https://atmos.nmsu.edu/PDS/data/PDS4/. Path to access the data of Perseverance: Mars2020>mars2020_meda>data_calibrated_env/ and the data of Insight: InSight> twins_bundle> data_calibrated）.

References

Banfield, D., Spiga, A., Newman, C., Forget, F., Lemmon, M., Lorenz, R., Murdoch, N., Viudez-Moreiras, D., Pla-Garcia, J., Garcia, R. F., Lognonné, P., Karatekin, Ö., Perrin, C., Martire, L., Teanby, N., Hove, B. V., Maki, J. N., Kenda, B., Mueller, N. T., . . . Banerdt, W. B. (2020). The atmosphere of Mars as observed by Insight. *NAT GEOSCI*, *13*(3), 190-198. https://doi.org/10.1038/s41561-020-0534-0

Belov, Y., Khlopov, G., Khomenko, S., Linkova, A., Rudnev, G., & Voitovych, O. (2012, 2012). Experimental study of small-scale fluctuations of refraction index in surface air.

Cahoy, K. L., Hinson, D. P., & Tyler, G. L. (2006). Radio science measurements of atmospheric refractivity with Mars Global Surveyor. *J. Geophys. Res*, *111*(E5), E05003-n/a. https://doi.org/10.1029/2005JE002634

Chen, W., Lovejoy, S., & Muller, J. P. (2016). Mars' atmosphere: The sister planet, our statistical twin. *J GEOPHYS RES-ATMOS*, *121*(20), 11,968-911,988. https://doi.org/10.1002/2016JD025211

Cheng, Y., & Brutsaert, W. (2005). Flux-profile relationships for wind speed and temperature in the stable atmospheric boundary layer. *BOUND-LAY METEOROL*, *114*(3), 519-538. https://doi.org/10.1007/s10546-004-1425-4

Davy, R., Davis, J. A., Taylor, P. A., Lange, C. F., Weng, W., Whiteway, J., & Gunnlaugson, H. P. (2010). Initial analysis of air temperature and related data from the Phoenix MET station and their use in estimating turbulent heat fluxes. *J. Geophys. Res*, *115*(E3), n/a. https://doi.org/10.1029/2009JE003444

Gheynani, B. T., & Taylor, P. A. (2011). Large Eddy Simulation of typical dust devil-like vortices in highly convective Martian boundary layers at the Phoenix lander site. *Planetary and Space Science*, *59*(1), 43-50. https://doi.org/10.1016/j.pss.2010.10.011

Haberle, R. M., Houben, H. C., Hertenstein, R., & Herdtle, T. (1993). A boundary-layer model for Mars - Comparison with Viking lander and entry data. *J ATMOS SCI*, *50*(11), 1544-1559. https://doi.org/10.1175/1520-0469(1993)050<1544:ABLMFM>2.0.CO2

Hogstrom, U. (1988). Non-dimensional wind and temperature profiles in the atmospheric surface layer: A re-evaluation. *BOUND-LAY METEOROL*, *42*(1-2), 55-78. https://doi.org/10.1007/BF00119875

Kelly, M., & Wyngaard, J. C. (2006). Two-dimensional spectra in the atmospheric boundary layer. *J ATMOS SCI*, *63*(11), 3066-3070. https://doi.org/10.1175/JAS3769.1

Larsen, S. E., Jørgensen, H. E., Landberg, L., & Tillman, J. E. (2002). Aspects of the atmospheric surface layers on Mars and Earth. *BOUND-LAY METEOROL*, *105*(3), 451-470. https://doi.org/10.1023/A:1020338016753

Lemmon, M. T., Wolff, M. J., Bell, J. F., Smith, M. D., Cantor, B. A., & Smith, P. H. (2015). Dust aerosol, clouds, and the atmospheric optical depth record over 5 Mars years of the Mars Exploration Rover mission. *ICARUS*, *251*, 96-111. https://doi.org/10.1016/j.icarus.2014.03.029

Martínez, G., Valero, F., & Vázquez, L. (2009). Characterization of the Martian surface layer. *J ATMOS SCI*, *66*(1), 187-198. https://doi.org/10.1175/2008JAS2765.1

Obukhov, A. M. (1971). Turbulence in an atmosphere with a non-uniform temperature. *Boundary-layer meteorology*, *2*(1), 7-29. https://doi.org/10.1007/BF00718085

Peng, Y., Zhang, L., Cai, Z., Wang, Z., Jiao, H., Wang, D., Yang, X., Wang, L., Tan, X., Wang, F., Fang, J., Sun, Z., Feng, H., Huang, X., Zhu, Y., Chen, M., Li, L., & Li, Y. (2020). Overview of the Mars climate station for Tianwenâ1 mission. *Earth and Planetary Physics*, *4*(4), 371-383. https://doi.org/10.26464/epp2020057

Petrosyan, A., Galperin, B., Larsen, S. E., Lewis, S. R., Määttänen, A., Read, P. L., Renno, N., Rogberg, L. P. H. T., Savijärvi, H., Siili, T., Spiga, A., Toigo, A., & Vázquez, L. (2011). THE MARTIAN ATMOSPHERIC BOUNDARY LAYER. *REV GEOPHYS*, *49*(3), RG3005-n/a. https://doi.org/10.1029/2010RG000351

Seiff, A., Tillman, J. E., Murphy, J. R., Schofield, J. T., Crisp, D., Barnes, J. R., LaBaw, C., Mahoney, C., Mihalov, J. D., Wilson, G. R., & Haberle, R. (1997). The atmosphere structure and meteorology instrument on the Mars Pathfinder lander. *J. Geophys. Res*, *102*(E2), 4045-4056. https://doi.org/10.1029/96JE03320

Smith, D. E., Zuber, M. T., Frey, H. V., Garvin, J. B., Head, J. W., Muhleman, D. O., Pettengill, G. H., Phillips, R. J., Solomon, S. C., Zwally, H. J., Banerdt, W. B., Duxbury, T. C., Golombek, M. P., Lemoine, F. G., Neumann, G. A., Rowlands, D. D., Aharonson, O., Ford, P. G., Ivanov, A. B., . . . Sun, X. (2001). Mars Orbiter Laser Altimeter experiment summary after the first year of global mapping of Mars. J. Geophys. Res, 106(E10), 23689-23722. https://doi.org/10.1029/2000JE001364

Wyngaard, J. C., Izumi, Y., & Collins, S. A. (1971). Behavior of the Refractive-Index-Structure Parameter near the Ground*. *Journal of the Optical Society of America*, *61*(12), 1646-1650. https://doi.org/10.1364/JOSA.61.001646

Ground Research and Application System of China's Lunar and Planetary Exploration Program. Mars Climate Station level 2C datasets. China National Space Administration, 2020. http://moon.bao.ac.cn